e-Navi

Available online at http://www.e-navigation.kr/
e-Navigation Journal

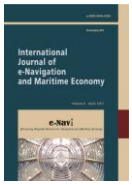

Original article

Effect of Cylinder Diameter on the Aerodynamic Characteristics of the Magnus Airfoil☆

Shilong Li [a], Haihua Lin [b], Chengmeng Sun[c*], Fei Cao[d]

[a] School of Naval Architecture and Port Engineering, Shandong Jiaotong University, Weihai 264209, China, 2715404128@qq.com

[b] School of Naval Architecture and Port Engineering, Shandong Jiaotong University, Weihai 264209, China, 7216219@qq.com

[c*] School of Naval Architecture and Port Engineering, Shandong Jiaotong University, Weihai 264209, China, scmeng717@163.com, Corresponding Author

[d] School of Naval Architecture and Port Engineering, Shandong Jiaotong University, Weihai 264209, China, 15106662723@163.com

Abstract

The Magnus airfoil can convert wind energy into kinetic energy, driving the boat forward. The rotating cylinder at the airfoil's leading edge enhances lift and reduces drag, positioning it as a promising technology for boundary layer flow control. This study, based on the NACA0015 airfoil, employs Computational Fluid Dynamics (CFD) to investigate the effect of cylinder diameter on the aerodynamic performance of the Magnus airfoil. The Reynolds number is set to 4×10^5, with an angle of attack of 18°, a rotational speed ratio of 1.4, and cylinder diameters ranging from 6% to 13% of the airfoil's chord length. Numerical simulations are conducted to analyze and compare the lift and drag characteristics, vorticity distribution, pressure distribution, and flow field structure for varying cylinder diameters. The results show that a high-speed rotating cylinder, when placed at the airfoil's leading edge, effectively suppresses flow separation on the suction surface, delays boundary layer development, and enhances the overall aerodynamic performance of the airfoil. For the Magnus airfoil studied, the optimal diameter of the rotating cylinder at the leading edge is found to be 12% of the chord length.

Keywords: Numerical Simulation; Rotating Cylinder; Magnus Airfoil; Aerodynamic Characteristics

https://doi.org/10.52820/j.enavi.2025.24.024

1. Introduction

In recent years, the global climate change situation and the challenges in environmental protection have become increasingly severe, and the international community has set higher requirements for greenhouse gas emission reduction in the shipping industry. To this end, the International Maritime Organization (IMO) has explicitly proposed the goal of achieving net-zero GHG emissions from the shipping industry by 2050 (2024). Against this backdrop, the research, development, and application of various energy-saving and emission-reduction technologies have become increasingly urgent. Marine sail technology (2022) is one such approach, which saves fuel consumption by converting wind energy into thrust.

In sail-assisted propulsion technology, Moving Surface Boundary-Layer Control (MSBC)is an emerging fluid control technology that modifies the boundary layer flow characteristics by applying moving boundary conditions on the surface of an object (1997). This can lead to reduced drag, delayed flow separation, postponed transition to turbulence, and potentially enhanced lift. MSBC technology is applied across various fields, including aerospace, wind power generation, and marine engineering. For example, Modi (1998) used MSBC by embedding a rotating cylinder into a spiral groove aligned with the axial direction, achieving better aerodynamic performance than cylinders on smooth or rough surfaces. Similarly, Zhang et al. (2024) embedded a rotating cylinder at the leading edge of a wing model simulating back-and-forth flapping motion, finding improved energy collection efficiency. In the design of ship wing sails, traditional fixed sails can harness wind power to propel the ship forward, but their performance is often limited in the dynamic and variable marine environment. The introduction of MSBC technology has brought significant advancements to the design and application of ship wing sails. By installing rotating cylinders or other forms of moving components on the wing sail's surface, momentum is injected into the boundary layer, effectively delaying flow separation, reducing drag, and potentially enhancing lift, which allows ships to utilize wind power more efficiently for propulsion. For instance, Deng Haoyun et al. (2023) investigated the thrust characteristics of a sailboat with a rotating cylinder and flap sail combination, finding that this combination significantly improved the propulsion efficiency of the ship.

This study focuses on the Magnus airfoil, which incorporates the MSBC technology mentioned above, with the goal of significantly enhancing its propulsion efficiency. The airfoil integrates the advantages of both a rotating cylinder and a baseline airfoil, resulting in an innovative design. The table below provides a detailed comparison of the lift-drag coefficients and lift-drag ratios for the baseline airfoil, the independent rotating cylinder (rotating sail), and the Magnus airfoil under their respective optimal operating conditions, all at the same Reynolds number. Since the optimal performance conditions vary for each of the three designs, the best conditions for each are specifically chosen as the basis for comparison, aiming to comprehensively highlight their performance differences.

Table 1. Comparison of three types of sails

Types of sails	Sail characteristics	Operating conditions	Lift coefficient
NACA0015 (2007)	No energy consumption.	Maximum angle of attack is 14°.	1.085
Rotating sail (2024)	High energy consumption.	Rotational speed ratio is 1.4.	3.75
Magnus airfoil	Low energy consumption, wide range of usable angles of attack.	Rotational speed ratio is 1.4, angle of attack is 18°.	1.3

As shown in the Table 1, the individual airfoil does not consume energy and has the lowest lift coefficient among the three types of sails. However, its usable angle of attack range is smaller compared to the Magnus airfoil. The Magnus airfoil demonstrates excellent aerodynamic performance, with a wide range of usable angles of attack and a delayed stall angle compared to the baseline airfoil. In terms of energy consumption, the

Magnus airfoil requires less energy due to the relatively small diameter of the rotating cylinder, typically around 10% of the chord length. Given these advantages, this study focuses on in-depth research on the Magnus airfoil.

The Magnus airfoil studied in this paper integrates a rotating cylinder at the leading edge of the baseline airfoil, utilizing the cylinder's rotation to enhance the airfoil's aerodynamic performance. As illustrated in Figure 1, the rotating cylinder induces the surrounding fluid to rotate, accelerating the fluid velocity on one side and injecting momentum into the airfoil's boundary layer. On the opposite side, the fluid velocity decreases (2023). According to Bernoulli's principle, an increase in fluid velocity results in a decrease in pressure, while a decrease in velocity leads to an increase in pressure. This creates a pressure difference across the rotating cylinder in the lateral direction, generating a lateral force, which, when combined with the force generated by the airfoil, further enhances lift.

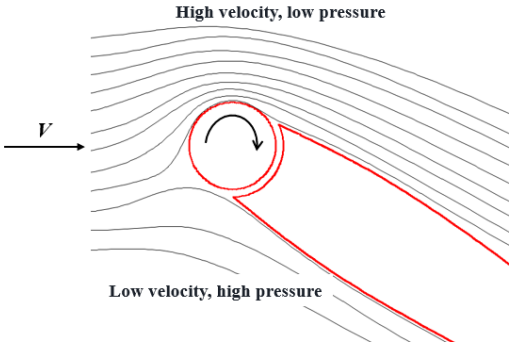

Figure 1. Diagram of the Magnus effect.

Extensive research has been conducted on the aerodynamic characteristics of independent rotating cylinders and airfoils, and the flow characteristics of the Magnus airfoil, formed by combining a rotating cylinder with an airfoil, have also been explored. Based on the symmetry of the airfoil, this combined structure is categorized into symmetric and asymmetric types. This part focuses on research progress regarding the aerodynamic performance of symmetric Magnus airfoil structures. Modi (2015) selected the Joukowsky airfoil, installed a rotating cylinder at its leading edge, and conducted wind tunnel experiments for validation. The results indicated that, compared to the baseline airfoil, the addition of the rotating cylinder significantly expanded the range of angles of attack that generate positive lift, increased the lift coefficient, and delayed the stall angle. Zhou et al. (2023) studied the NACA0012 airfoil, similarly installing a rotating cylinder at its leading edge and experimentally validating the effect of the rotating cylinder on the NACA 0024 airfoil. In addition, they examined the influence of airfoil thickness on aerodynamic performance, finding that as airfoil thickness increased, drag also significantly increased. Therefore, an optimal balance between lift and drag can only be achieved by selecting the appropriate airfoil thickness. The studies by Al-Garni (2000) and Aktharuzzaman (2017) further substantiated the significant impact of the leading-edge rotating cylinder in increasing the lift coefficient and delaying the stall angle. Al-Garni et al. also found that when the flap at the trailing edge of the airfoil was deflected, it could improve lift, but also reduce the lift-to-drag ratio. Aktharuzzaman’s et al. experimental research was more comprehensive, examining the effects of the rotating cylinder's position, speed, and surface conditions on aerodynamic performance, and providing many valuable conclusions. Additionally, Salam's et al. (2019) research revealed the significant effect of the rotational speed ratio of the rotating cylinder on the aerodynamic performance of the airfoil. When the rotational speed ratio of the rotating cylinder exceeded 0.356 and 0.7, both the lift and drag characteristics of the NACA 0021 airfoil were significantly improved. This is because the momentum injection of the rotating cylinder enhanced the suction on the upper surface of the airfoil, thereby increasing the lift coefficient.

In the exploration of the aerodynamic characteristics of asymmetric Magnus airfoil structures, Mohamed (2020) and Zhuang Yueqing (2011) were the first to conduct numerical simulations. They installed a rotating cylinder at the leading edge of the S809 airfoil and found a significant increase in the lift-to-drag ratio. By rotating the leading-edge cylinder, they effectively suppressed flow separation on the suction side, improving the airfoil's aerodynamic performance at higher angles of attack. Salimipour et al. (2024) employed a similar approach by installing a movable surface on the S809 airfoil, confirming that this surface also enhanced the lift-to-drag ratio and suppressed vortex street formation. Zhou et al. had already conducted in-depth research on the effects of symmetric airfoil thickness. Building on this work, Salam (2020) investigated the impact of asymmetric airfoil thickness through experimental research. They installed a rotating cylinder with a low rotational speed ratio at the leading edge of the

asymmetric NACA23018 airfoil and observed its effect on the formation of Kármán vortex streets. The results showed that the rotating cylinder not only regulated the flow field around the airfoil but also suppressed vortex street formation, thereby improving the lift-to-drag ratio and delaying stall. Yahiaoui et al. (2015) further confirmed these findings through numerical simulations, observing similar aerodynamic improvements when a rotating cylinder was installed at the leading edge of the NACA 63218 airfoil. KB et al. (2024) selected the NACA2412 airfoil and installed a rotating cylinder at its leading edge. Numerical simulations revealed significant variations in the optimal cylinder rotational speed ratios at different angles of attack. Based on these studies, Gada et al. (2016) proposed that when the speed of the rotating cylinder matches or exceeds twice the free stream velocity, the lift-to-drag ratio could be improved by approximately 10%.

Whether for symmetric or asymmetric Magnus airfoil structures, installing a rotating cylinder at the leading edge of the airfoil yields favorable results. Further studies have shown that positioning the rotating cylinder at the back or trailing edge of the airfoil can also optimize its aerodynamic performance. Modi pointed out that installing a rotating cylinder at the trailing edge behaves similarly to a flap, significantly increasing the lift coefficient before reaching stall conditions. Lou et al. (2020) proposed that embedding a rotating cylinder at the back of the airfoil could suppress flow separation at the rear and improve the airfoil's aerodynamic stability, also expanding its operational range. Shan Jixiang et al. (2017)found that adding a rotating cylinder to the trailing edge of the airfoil increased both the drag and lift coefficients, but significantly reduced the pitching moment coefficient. They also explored the effect of rotational speed ratio and found that while the lift-to-drag ratio increased with the rotational speed ratio, the rate of increase gradually slowed. Zhang et al. (2023) also studied the aerodynamic performance of embedding a rotating cylinder at the tail of the airfoil, with the unique addition of considering the direction of cylinder rotation. They found that clockwise rotation improved the lift coefficient and delayed the flow separation point, while counterclockwise rotation produced the opposite effect.

In the previous discussion of the aerodynamic performance of symmetric Magnus airfoil structures, the influence of airfoil thickness was mentioned. In fact, other parameters, such as the rotational speed ratio, diameter, gap, and position, also play significant roles in determining the aerodynamic performance of the airfoil. To this end, Zhang et al. (2010) employed Computational Fluid Dynamics (CFD) techniques to thoroughly investigate the impact of several of these parameters, optimizing the design to achieve the best lift-to-drag ratio. They compared the numerical simulation results with experimental data and found that the optimized airfoil had a higher lift coefficient and maintained good aerodynamic performance even at higher angles of attack. Tang Xinzi et al. (2021) systematically examined the effects of rotational speed ratio, gap, and position on the boundary layer flow and lift-to-drag ratio under low Reynolds number conditions. They developed a nonlinear response model based on Latin hypercube sampling and Kriging methods to analyze the relationship between the rotational speed ratio, gap, and position, and the airfoil's lift-drag characteristics. Their analysis quantified the influence of the Magnus effect and determined the optimal parameter values under specific conditions. Additionally, Zhang Ling et al. (2018) studied a combined airfoil with a leading-edge rotating cylinder and NACA0015, while Gong Zhibin et al. (2015) used another airfoil as a subject for investigation. Both conducted numerical simulations to explore the effects of parameters such as cylinder rotational speed ratio, the gap between the cylinder and the airfoil, and the position of the cylinder on the aerodynamic performance of the combined airfoil.

To present these research findings more clearly, the results are summarized below in the table, organized by research direction, content, and findings.

Table 2. Research findings summary

Research direction	Research content	Research conclusion
Installation of a Rotating Cylinder at the Leading Edge of a Symmetric Airfoil.	Joukowsky, NACA 00 series airfoils.	Increase the maximum lift coefficient and delay the stall angle.
Installation of a Rotating Cylinder at the Leading Edge of an Asymmetric Airfoil.	NACA23018, NACA 63218, NACA2412, S809 airfoils.	
Optimization of Key Parameters for the Magnus Airfoil.	Rotational speed ratio, cylinder-to-airfoil gap, cylinder center position.	Improve the airfoil performance by optimizing its parameters.
Installation of the cylinder at other locations on the airfoil.	Cylinder installed on the trailing edge or rear surface of the airfoil.	Increase the lift coefficient at low angles of attack.

The academic community has made significant progress in researching the aerodynamic characteristics of the Magnus airfoil, specifically the combination of a rotating cylinder and an airfoil. Scholars have studied the aerodynamic performance of rotating cylinders on both symmetric and asymmetric airfoils and have also examined the effects of the cylinder's center position at various locations on the airfoil. Moreover, some researchers have analyzed how the geometric parameters of the structure critically impact the airfoil's overall performance. However, while extensive research has been conducted, the relationship between the cylinder diameter and the airfoil chord length, and its deep influence on aerodynamic performance, remains underexplored and warrants further investigation.

Building on previous research, this study uses numerical simulation techniques to focus on the critical factor of the rotating cylinder diameter at the leading edge, analyzing its impact on the aerodynamic performance of the airfoil. Specifically, this study will provide a comprehensive and detailed analysis of the lift-drag characteristics, vorticity distribution, pressure distribution, and streamlines. By doing so, the study aims to reveal how changes in cylinder diameter affect lift generation, drag characteristics, vortex structure, and flow field dynamics, providing a stronger theoretical and scientific foundation for the optimization of Magnus airfoil design.

2. Numerical Methods and Physical Models

2.1 Air Resistance

In the simulation of the Magnus airfoil, air is considered as the working fluid, and the flow is assumed to be two-dimensional and incompressible, allowing the energy conservation equation to be neglected. The Navier-Stokes equations include the mass conservation equation and the momentum conservation equation:

$$\frac{\partial u}{\partial x}+\frac{\partial v}{\partial y}=0 \tag{1}$$

$$\rho\frac{\partial u}{\partial t}+\rho\nabla\cdot(u\boldsymbol{u})=X-\frac{\partial p}{\partial x}+\frac{\partial \tau_{xx}}{\partial x}+\frac{\partial \tau_{yx}}{\partial y} \tag{2}$$

$$\rho\frac{\partial v}{\partial t}+\rho\nabla\cdot(v\boldsymbol{u})=Y-\frac{\partial p}{\partial y}+\frac{\partial \tau_{xy}}{\partial x}+\frac{\partial \tau_{yy}}{\partial y} \tag{3}$$

where, x and y represent the downstream and transverse directions, respectively. u and v represent the components of the velocity vector in the x and y directions, respectively. ρ is the fluid density. t is time. $\nabla\cdot$ is the divergence of the velocity field. u is the velocity vector. p is the pressure. τ denotes the viscous stress. X and Y represent the body forces in the x and y directions, respectively.

2.2 Physical Models and Computational Domai

In the present study, the *SST k-ω* turbulence model, implemented in ANSYS/Fluent, is used for two-dimensional numerical simulations to investigate the aerodynamic performance of the Magnus airfoil. This turbulence model combines the advantages of both the *k-ε* and *k-ω* models, providing good accuracy and stability across a range of flow regimes. Additionally, the sliding mesh technique is employed to model the motion of the rotating cylinder.

The NACA0015 airfoil is selected as the base airfoil, with a cylinder added to the leading edge, creating the Magnus airfoil by combining it with the baseline airfoil. The leading edge is defined as the windward side, the upper surface is the suction side, and the lower surface is the pressure side. The main geometric parameters

include the chord length, cylinder diameter, and the gap distance between the cylinder and the airfoil, as shown in Figure 2. The leading edge point of the Magnus airfoil corresponds to the original baseline airfoil's leading edge, and after the addition of the rotating cylinder, the chord length remains unchanged. The chord length is the distance between the leading edge and trailing edge, denoted as *C*; the cylinder diameter is denoted as *D*; the gap distance between the rotating cylinder and the baseline airfoil is denoted as *d*; the rotational speed ratio is the ratio of the rotating cylinder's tangential velocity to the incoming flow velocity, denoted as V_R; the angle of attack, α, is the angle between the incoming flow direction and the airfoil's chord line.

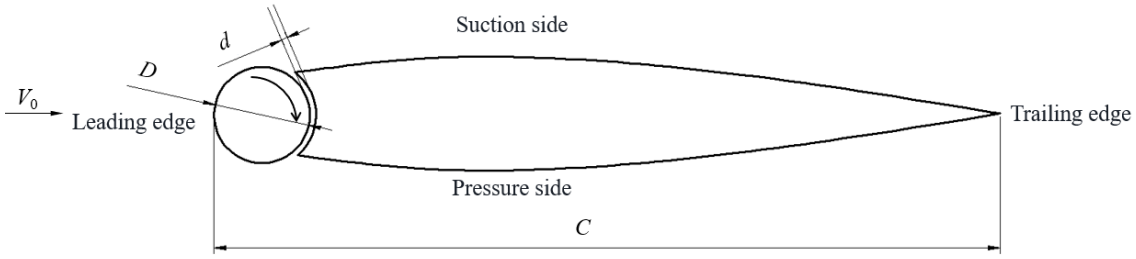

Figure 2. Geometric parameters of Magnus airfoil.

The computational domain and boundary conditions are shown in Figure 3 The direction of the incoming flow is along the positive x-axis. The total length of the computational domain is 32*C*, and the total width is 24*C*. The distance from the airfoil position to the inlet boundary condition is 12*C*, and the distance to the outlet boundary condition is 20*C*. The left side of the airfoil and both upper and lower sides are defined as velocity inlets, while the right side is defined as a pressure outlet. Both the cylinder surface and the airfoil surface are modeled as no-slip walls.

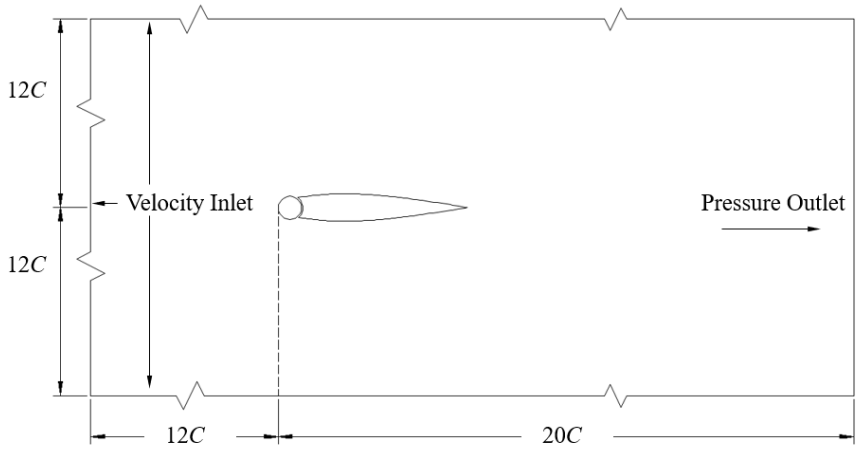

Figure 3. Compute domain and boundary conditions.

In the numerical simulation, the chord length C = 0.4 m, the uniform incoming flow velocity V_0 =15 m/s, and the fluid is air with a density of ρ = 1.225 kg/m3, Re = 4 × 10^5, where the kinematic viscosity μ = 1.7894×10−5 m²/s. The lift coefficient (C_L), drag coefficient (C_D), pressure coefficient (C_P), and lift-to-drag ratio (R_{AT}) are defined as follows:

$$C_L = \frac{F_L}{\frac{1}{2}\rho V_0^2 A} \tag{4}$$

$$C_D = \frac{F_D}{\frac{1}{2}\rho V_0^2 A} \tag{5}$$

$$C_P = \frac{P - P_\infty}{\frac{1}{2}\rho V_0^2} \tag{6}$$

$$R_{AT} = \frac{C_L}{C_D} \tag{7}$$

where: F_L represents the lift force, F_D represents the drag force, P denotes the total pressure at the point of interested, P_∞ represents the free stream pressure at the inlet of the computational domain, and their units are N ;A is the frontal area, unit is m^2.

2.3 Grid Generation and Numerical Validation

To further validate the grid convergence used in this study, grid convergence calculations were performed for a Reynolds number of 4×105 and an angle of attack of 6°. The boundary layer was discretized with y+≤1, and the first grid layer had a height of 0.02 mm. Lift and drag coefficients were computed for five different grid numbers. The results are presented in Table 3.

Table 3. Mesh convergence validation

Mesh	Number (ten thousand)	C_L	C_D
1	5.1	0.5843	0.01650
2	7.7	0.5858	0.01654
3	11.5	0.5866	0.01653
4	17.3	0.5868	0.01654
5	25.8	0.5867	0.01648

The results indicate that when the grid number increases from mesh1 to mesh3, the lift coefficient exhibits a slight increase. Further refinement leads to negligible changes in the lift coefficient, with fluctuations as small as 0.05%. The drag coefficient shows negligible variation with changes in grid number. Therefore, to balance computational efficiency and accuracy, a grid model with mesh3 is used for the simulations.

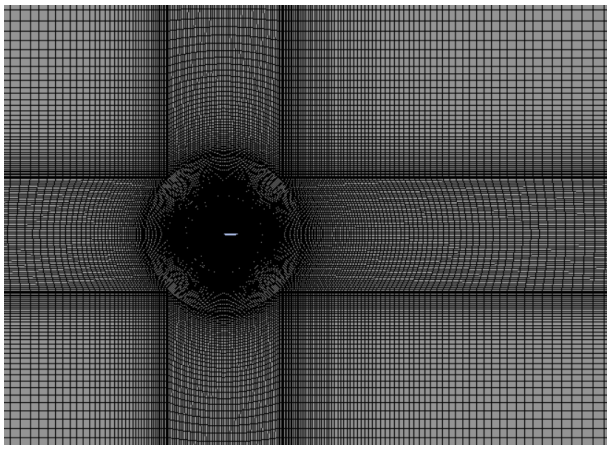

(a) Overall Grid

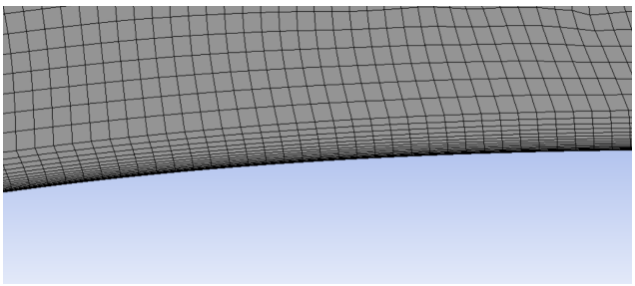

(b) Local mesh

Figure 4. Computational mesh

As shown in Figure 4, the mesh division results of the computational model. To accurately capture the influence of boundary layer variations on the lift and drag coefficients, the mesh is refined near the airfoil surface for accuracy, and coarsened further away from the airfoil to reduce computational cost.

To assess the accuracy and feasibility of the numerical method, the lift and drag coefficient curves for the NACA0015 airfoil are shown in FIG. 5, and compared with the experimental data from Chen Li . The incoming flow velocity is resolved into components along the *x* and *y* directions. By adjusting these components, the resultant velocity is maintained at a constant 15 m/s, with the direction corresponding to the required angle of attack for the simulation. This approach allows for simulations at different angles of attack by adjusting the velocity components.

As shown in Figure 5, the numerical simulation results are in good agreement with the experimental data within the angle of attack range from 0° to 14°. However, when the angle of attack exceeds 14°, a significant discrepancy emerges between the numerical and experimental results. This discrepancy arises because, at higher angles of attack, the flow separation point shifts closer to the leading edge of the airfoil, increasing the risk of stall, which may occur. At this point, the flow over the upper surface of the airfoil becomes increasingly unstable, leading to a greater discrepancy between the computational results and the experimental observations. Therefore, it can be reasonably concluded that the numerical simulation is highly reliable up to the stall angle.

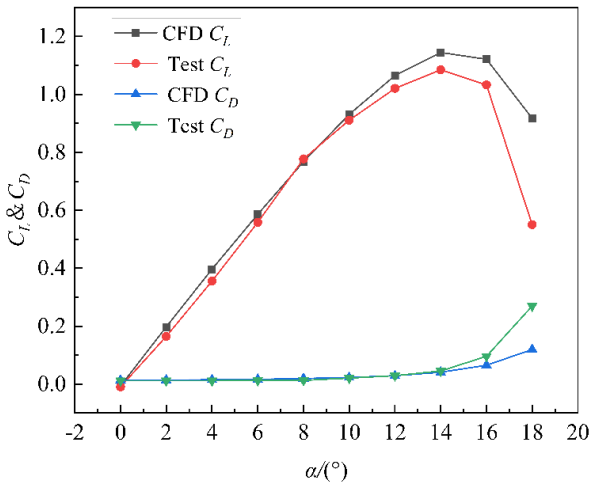

Figure 5. Numerical validation comparison chart.

3. Analysis of the Effect of Cylinder Diameter on Airfoil Aerodynamic Characteristics

Based on the numerical validation results discussed above, the NACA0015 airfoil reaches its highest lift coefficient at an angle of attack of 14° and then stalls. Therefore, for the study of the airfoil with a leading-edge rotating cylinder, this paper selects an angle of attack of 18°—at which stall has already occurred—for numerical simulations. This allows for the exploration of the performance of this special design under extreme conditions. Specifically, the study uses an angle of attack α of 18°, with a Reynolds number of Re=4×10^5, a gap d=0.7mm, and a Magnus airfoil chord length C=400mm. The incoming flow velocity V_0 is 15 m/s, and the rotational speed ratio V_R is fixed at 1.4. The cylinder diameter D is varied from 6% to 13% of C, with calculations performed for each 1% increment of C, corresponding to diameters ranging from 24 mm to 52 mm. This methodology enables a comprehensive evaluation of the performance differences for different cylinder diameters.

3.1 Lift and Drag Analysis

Figure 6 presents the lift-to-drag characteristics of the airfoil for cylinder diameters of 6% C, 7% C, 8% C, 9% C, 10% C, 11% C, 12% C, and 13% C.

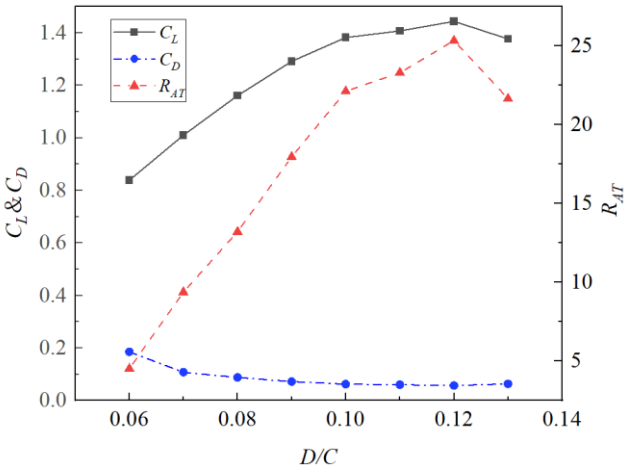

Figure 6. Lift and drag values for different cylinder diameter

The lift coefficient curve shows that as the cylinder diameter increases, the lift coefficient C_L initially rises rapidly and then decreases gradually. Overall, the lift coefficient increases significantly within this range. When the cylinder diameters are 6% C and 12% C, the lift coefficients are 0.839 (minimum) and 1.4437 (maximum), respectively, indicating that increasing the cylinder diameter significantly enhances the lift coefficient under certain conditions. Further analysis reveals that within the studied range, the lift coefficient is positively correlated with the cylinder diameter. From 6% to 10% C, the lift coefficient increases rapidly, while between 10% and 12% C, the increase slows down. When the cylinder diameter increases from 12% C to 13% C, the lift coefficient decreases. This can be attributed to the cylinder diameter's impact on the alignment with the airfoil leading edge shape. At 12% C, the rotating cylinder aligns most effectively with the airfoil leading edge, improving flow characteristics and enhancing boundary layer control. However, when the diameter increases to 13% C, the excessive size disrupts the leading edge shape, affecting the boundary layer development and causing a decrease in the lift coefficient.

The drag coefficient curve shows the opposite trend to the lift coefficient: as the cylinder diameter increases, the drag coefficient C_D decreases initially and then increases slowly. Compared to the lift coefficient, the drag coefficient remains relatively stable across a broader range, with smaller changes. When the cylinder diameters are 6% C and 12% C, the drag coefficients are 0.1855 (maximum) and 0.05698 (minimum), respectively, suggesting that increasing the cylinder diameter can reduce the drag coefficient. Although the variation in drag coefficient is similarly significant, the actual impact is smaller due to the lower absolute values. The drag coefficient variation is mainly influenced by the flow separation point. When the cylinder diameter is 6% C, the flow separation point is closer to the leading edge, resulting in a higher drag coefficient. As the diameter increases, the Magnus effect generated by the rotating cylinder suppresses flow separation, moving the separation point downstream and reducing the drag coefficient. The separation point is closest to the trailing edge when the diameter is 12% C, minimizing the drag coefficient. However, at 13% C, the impact of the rotating cylinder.

The variation in the lift-to-drag ratio reflects the trends of the lift and drag coefficients, showing an initial increase followed by a decrease. When the cylinder diameter is 12% C, the lift-to-drag ratio reaches its peak, with the lift coefficient being relatively high and the drag coefficient being low, resulting in the best aerodynamic

efficiency for the airfoil. Furthermore, within the diameter range of 10%–12% *C*, the lift-to-drag ratio remains above 22, indicating that the positive effects of the rotating cylinder are fully utilized, leading to excellent aerodynamic performance. However, when the cylinder diameter is further increased to 13% *C*, the lift coefficient decreases and the drag coefficient increases, causing a noticeable drop in the lift-to-drag ratio. This suggests that excessively large cylinder diameters negatively impact the overall aerodynamic performance of the airfoil.

In conclusion, the cylinder diameter has a significant effect on the aerodynamic characteristics of the airfoil, with the optimal diameter being 12% *C*. At this diameter, the separation point is located closest to the trailing edge, the separation region is minimized, the lift coefficient reaches its maximum, and the drag coefficient reaches its minimum, resulting in the peak lift-to-drag ratio.

3.2 Vortex shedding analysis

The aerodynamic variations in the lift coefficient, drag coefficient, and lift-to-drag ratio of the Magnus airfoil can be explained through the vorticity maps. Figure 7 shows the vorticity maps of the Magnus airfoil for different cylinder diameters.

As shown in Figure 7, the vorticity distribution varies significantly with changes in cylinder diameter, particularly in terms of the wake's length, width, and morphological characteristics. In general, as the cylinder diameter increases from 6% *C* to 12% *C*, the wake shortens and the width of the wake region decreases. This trend aligns with the continuous increase in the lift coefficient, indicating that the wake's length and width play an important role in the Magnus airfoil's aerodynamic characteristics, and are negatively correlated with the lift-to-drag ratio.

When the cylinder diameter is 6% *C*, the Kármán vortex street in the wake is more distinct, indicating that flow separation is severe, and vortex shedding is strong. This periodic variation in vorticity weakens the Magnus effect, resulting in a lower lift coefficient. The main reason is that at this point, the cylinder diameter is small, and the Magnus effect is weak, unable to significantly affect the boundary layer characteristics, failing to suppress flow separation and vortex instability.

For cylinder diameters in the range of 7% to 12% *C*, the Kármán vortex street disappears, and the wake's unsteadiness is significantly reduced. A steady wake gradually dominates the wake region behind the airfoil. At this point, the wake becomes long, narrow, and gradually diffuses, resembling a comet tail. This phenomenon suggests that as the cylinder diameter increases, the rotating cylinder injects sufficient momentum into the boundary layer, suppressing flow separation, reattaching the boundary layer to the suction surface, and enhancing resistance to the adverse pressure gradient. Meanwhile, the area of the steady wake region shrinks, and the flow field becomes more symmetric. The vortex strength in the wake becomes moderate, and the vortex shedding frequency decreases, leading to a significant improvement in aerodynamic performance. This steady-state flow significantly reduces the drag coefficient, making the pressure distribution more favorable for lift generation, thus increasing the lift coefficient. During this phase, the airfoil demonstrates higher aerodynamic efficiency, and the lift-to-drag ratio increases. When the cylinder diameter is 12% *C*, the wake region is minimized, and the separation point is furthest downstream, yielding the best aerodynamic performance for the airfoil, indicating an optimal balance between the cylinder diameter and airfoil size.

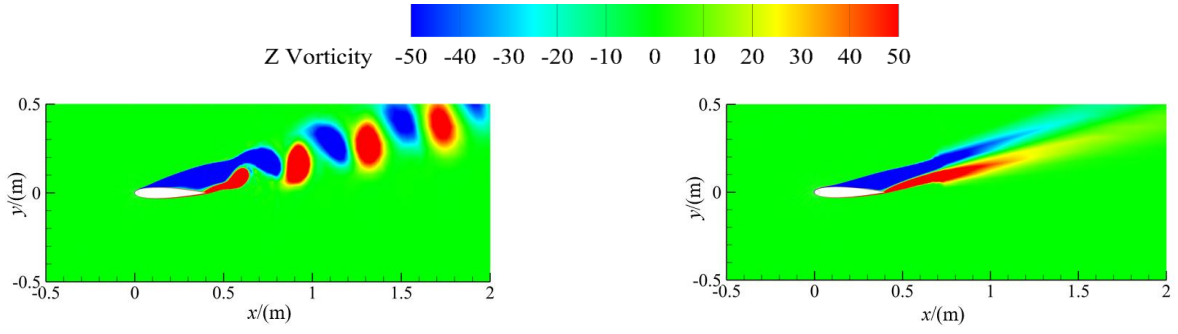

6%*C* 7%*C*

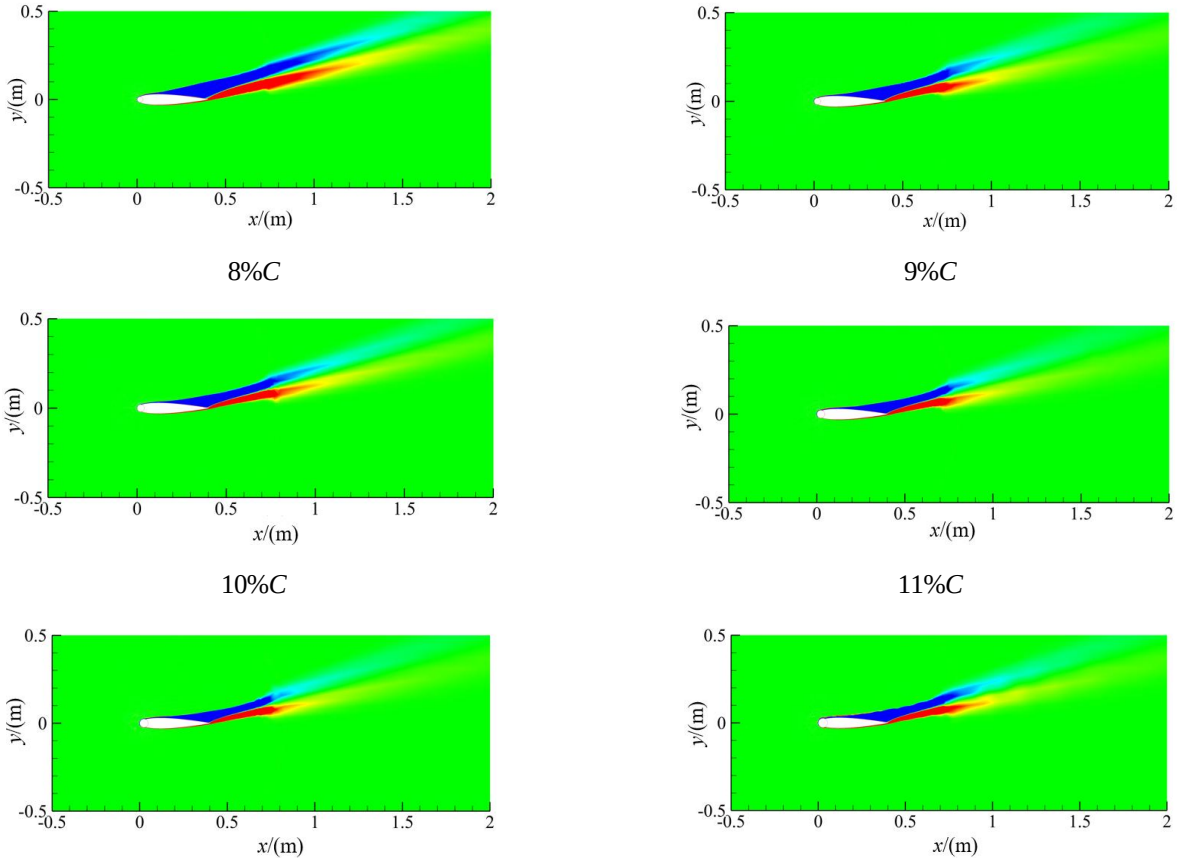

Figure 7. Vorticity Patterns of Magnus Airfoils with Different Cylinder Sizes

However, when the cylinder diameter increases to 13% *C*, the wake region expands compared to 12% *C*, as the larger diameter disrupts the optimal balance between the cylinder and airfoil size. This leads to a re-establishment of flow separation, with the vortex becoming unstable, weakening the Magnus effect.

In summary, when the cylinder diameter is small (e.g., 6% *C*), the shedding of the tail vortex causes strong disturbances in the flow field, increasing the viscous drag and resulting in a higher drag coefficient. At intermediate diameters (7%–12% *C*), the tail vortex gradually stabilizes, and the flow separation point moves toward the trailing edge of the airfoil, leading to a decrease and relative stabilization of the drag coefficient. However, at large diameters (13% *C*), the separation point moves upstream, the separation region expands, and the drag coefficient increases while the lift coefficient decreases. In conclusion, the interaction between the vortex and the airfoil is complex. Under different rotating cylinder diameters, the Magnus effect significantly affects the wake vortex structure, directly influencing the aerodynamic characteristics of the airfoil by altering the vorticity distribution and flow state. Particularly in the 8%–12% *C* diameter range, the wake exhibits better steady-state characteristics, resulting in higher lift coefficients and lower drag coefficients, which indicates improved aerodynamic performance. Among these, when the rotating cylinder diameter is 12% of the airfoil's chord length, the interaction between the vortex and the airfoil is most harmonious, producing stable and efficient lift, leading to the best aerodynamic performance for the Magnus airfoil.

3.3 Pressure coefficient curve analysis

The tail vortex characteristics of the Magnus airfoil have a direct impact on its aerodynamic performance, which is reflected in the pressure distribution acting on the airfoil. This, in turn, manifests in unique aerodynamic changes through parameters such as the lift coefficient, drag coefficient, and lift-to-drag ratio. To further investigate the effect of rotating cylinder size on the aerodynamic characteristics of the Magnus airfoil, FIG. 8 shows the distribution of the pressure coefficient on the airfoil surface for different cylinder diameters. The pressure coefficient distribution reflects the changes in fluid pressure along the airfoil surface. The upper branch of the curve corresponds to the suction side, while the lower branch corresponds to the pressure side.

The area enclosed by these two branches is strongly correlated with the lift coefficient: the larger the area, the greater the pressure difference and the higher the lift coefficient. By analyzing the shape and variation of the curve, we gain insight into how the rotating cylinder influences the airfoil's flow characteristics.

As shown in the figure, under the influence of the rotating cylinder, a high negative pressure peak forms on the suction side at the cylinder location. This is a direct manifestation of the Magnus effect. As the rotating cylinder spins rapidly, the relative motion between the cylinder surface and the incoming flow induces asymmetric boundary layer behavior. This leads to an increase in flow speed and a decrease in pressure on the upper surface, while the lower surface experiences a decrease in flow speed and an increase in pressure. This asymmetric pressure distribution generates lift. As the cylinder diameter increases from 6% *C* to 12% *C*, the Magnus effect strengthens, causing the local flow speed on the suction side to increase, which reduces the pressure and delays the separation point. At 6% *C*, the Magnus effect is weak, and the pressure curve area is the smallest. As the diameter increases to 7-9% *C*, the Magnus effect intensifies, and the flow asymmetry increases, moving the separation point downstream and increasing the negative pressure peak. When the cylinder diameter reaches 10% *C*, the negative pressure peak rises to nearly -8, and the lift coefficient continues to increase. When the cylinder diameter exceeds 10% *C*, the pressure distribution characteristics change. The width of the suction side curve at the cylinder location continues to increase, indicating that the Magnus effect is still in play. However, the negative pressure peak stabilizes around -8. As the diameter further increases to 13% *C*, the negative pressure peak decreases, and the separation point moves upstream, enlarging the separation region and increasing the suction surface pressure. This results in a decrease in the overall lift coefficient.

In summary, as the cylinder diameter increases from 6% to 12% *C*, the Magnus effect becomes stronger, and the local flow speed on the suction side increases, leading to a decrease in pressure and a delayed separation point. However, when the diameter increases beyond 12% *C*, the Magnus effect becomes less effective, and the separation point moves upstream, reducing the lift coefficient and weakening the lift enhancement effect.

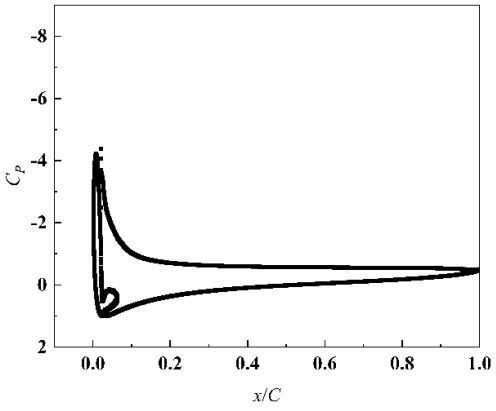

6%*C*

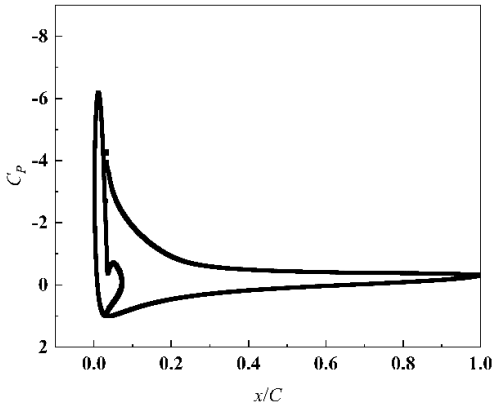

7%*C*

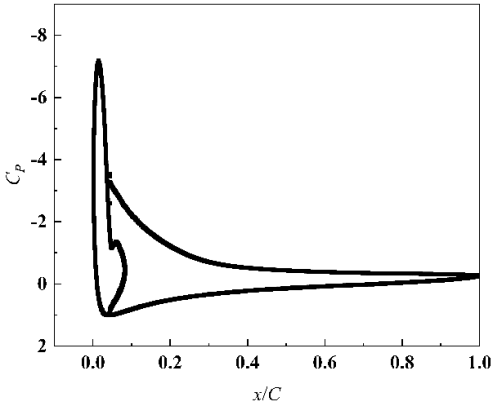

8%*C*

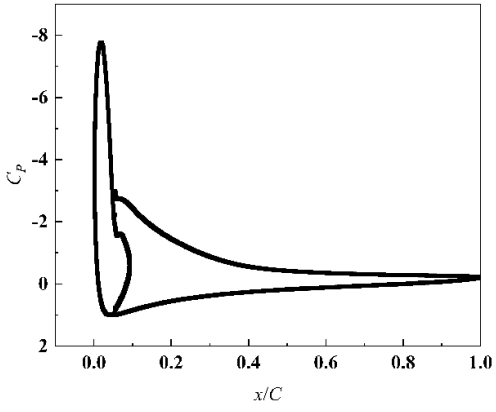

9%*C*

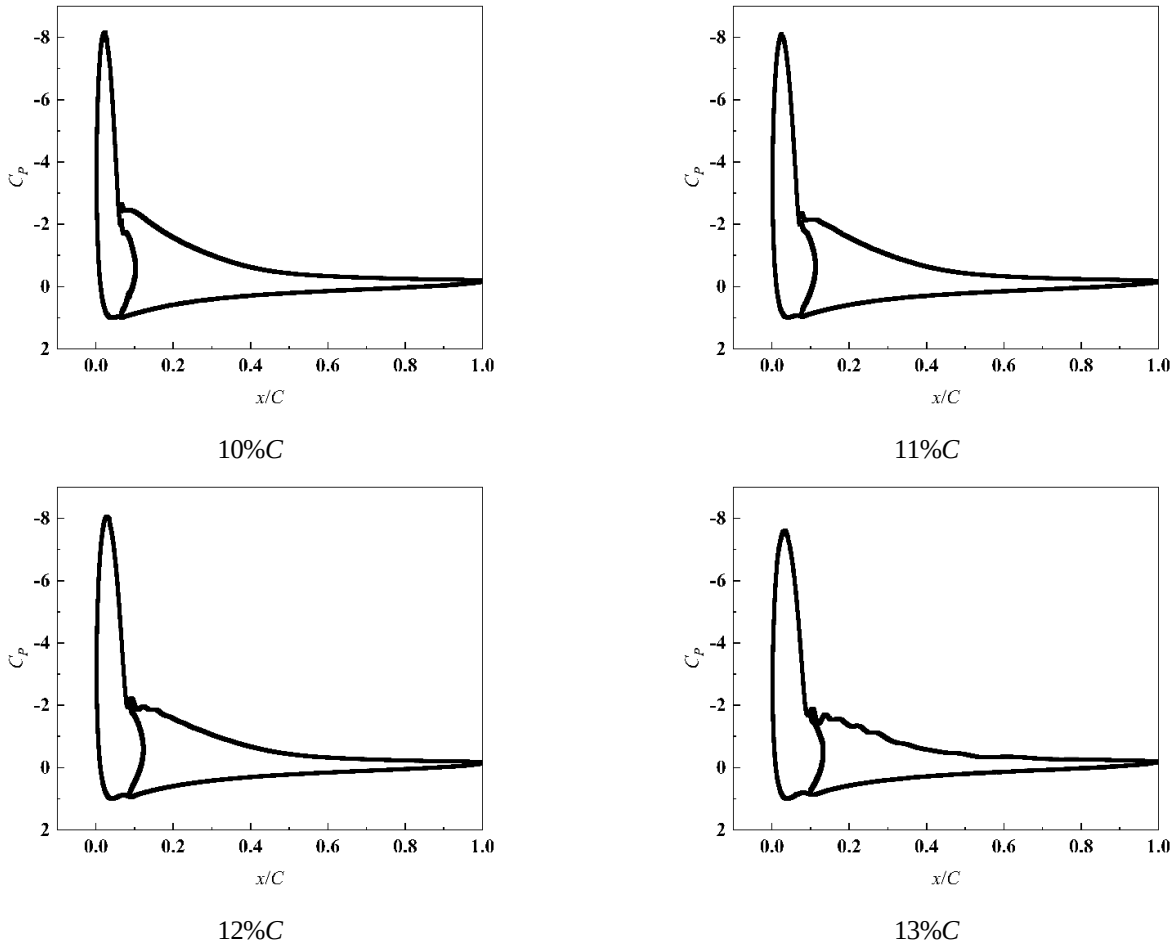

Figure 8. Pressure Coefficient Curves of Magnus Airfoils with Different Cylinder Sizes

3.4 Streamline analysis

To visually present the flow state of the Magnus airfoil's flow field, including flow direction, vortices, separation, and other complex flow phenomena, Figure 9 shows the streamline plots of the Magnus airfoil under different cylinder diameters.

As shown in Figure 9, the effect of different rotating cylinder sizes on the wake streamlines of the Magnus airfoil is illustrated. The streamline plot clearly reveals the flow separation behavior on the rear half of the suction side and its impact on the aerodynamic performance of the airfoil. The rotating cylinder significantly alters the flow field characteristics through the Magnus effect, with its enhanced rotational effect suppressing flow separation and improving the wake structure.

When the cylinder diameter is 6% *C*, a large flow separation region is observed on the rear half of the suction side, and strong disturbances at the tail lead to an unstable wake region and the formation of a Kármán vortex street behind the airfoil. The separation point is near the airfoil leading edge, which destabilizes the low-pressure region, increases lift loss, and raises drag. Therefore, at smaller cylinder diameters, the airfoil's aerodynamic performance is suboptimal.

As the cylinder diameter increases to 7% *C*, flow separation improves. The separation point shifts downstream, closer to the trailing edge compared to the 6% *C* cylinder diameter. The separation region at the rear of the airfoil reduces, and the tail disturbance region gradually disappears, resulting in a more stable, steady-state wake. This improvement in wake stability leads to a slight increase in the lift coefficient and a decrease in the drag coefficient.

In the range of cylinder diameters from 8% *C* to 11% *C*, further increasing the diameter to 8% *C* further reduces the separation region on the suction surface, with the separation point moving downstream. The wake flow becomes smoother, and the separation vortex size decreases, indicating that the Magnus effect strengthens further. This suppresses flow separation, enhances boundary layer control, and improves aerodynamic performance. As the diameter increases, the separation region continues to shrink and move downstream. At this point, the steady wake becomes highly stable, and

the wake region shortens significantly. The Magnus effect strengthens, delaying the boundary layer separation point and improving the attachment of the boundary layer to the airfoil surface, leading to a gradual increase in the lift coefficient and a decrease in the drag coefficient.

When the cylinder diameter reaches 12% *C*, the aerodynamic characteristics of the airfoil are optimal. At this diameter, the separation area on the rear half of the suction surface is minimized, and the separation point is furthest downstream. The wake region shows a stable steady-state flow field, indicating that the Magnus effect and flow dynamics have reached an optimal balance. This results in the maximum lift coefficient, the minimum drag coefficient, and significant improvements in aerodynamic efficiency.

However, when the cylinder diameter increases to 13% *C*, the flow separation region expands again, and the separation point moves upstream, causing the separation vortex to re-strengthen. The increased wake region leads to a decrease in the lift coefficient, an increase in the drag.

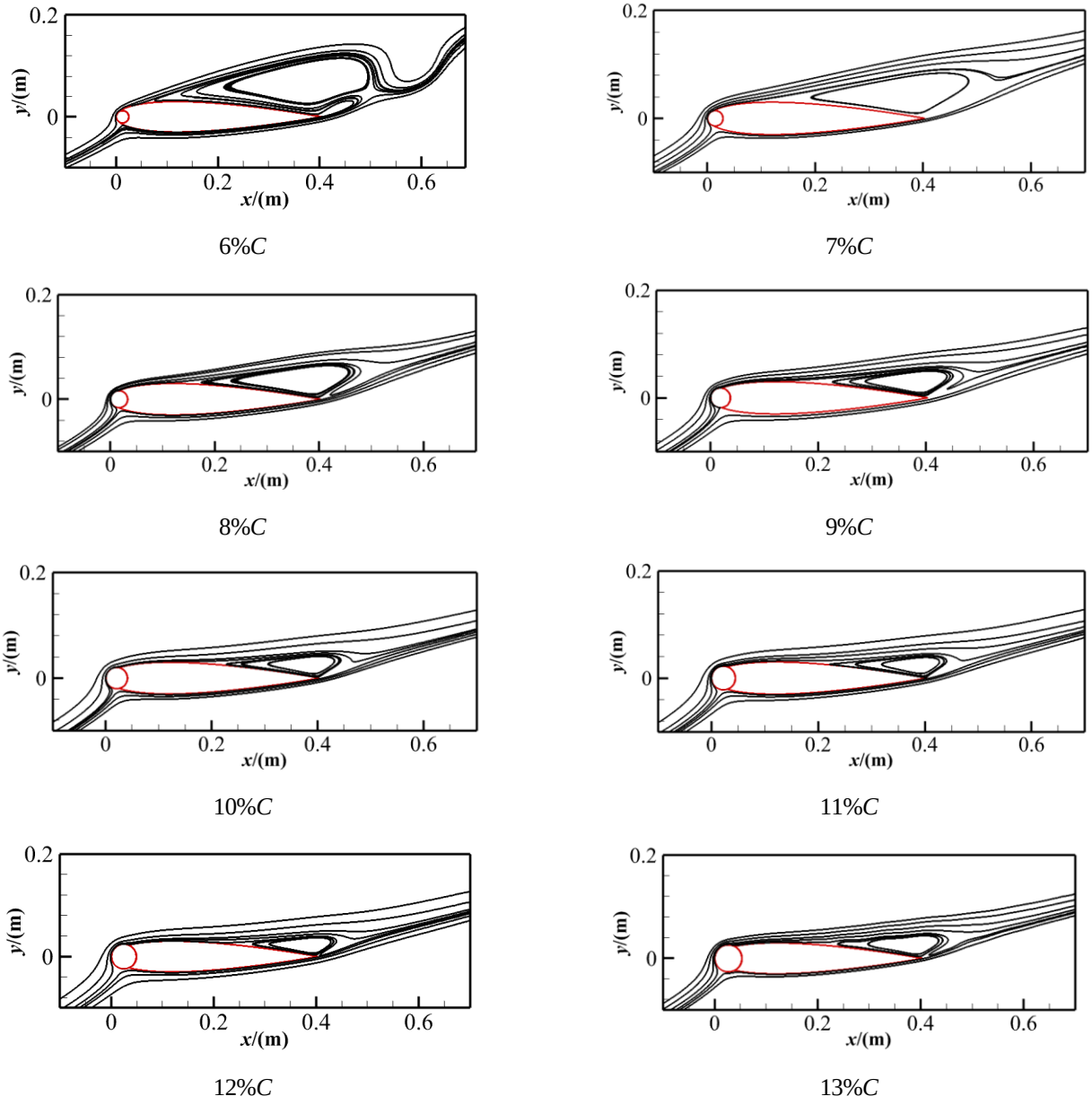

Figure 9. Streamline diagrams of Magnus airfoils with different cylinder diameters

In summary, by applying a rotating cylinder at the leading edge of the airfoil, the Magnus effect can effectively suppress flow separation on the airfoil surface and optimize the flow field structure. However, this effect is influenced by the cylinder size. When the cylinder diameter is 12% *C*, the aerodynamic performance is optimal, with the rotating cylinder achieving the best balance in suppressing separation, improving the wake, and reducing drag.

3.5 Velocity analysis above the airfoil

Based on the previous analysis, it can be seen that the cylinder diameter has a significant impact on the flow field generated by the Magnus airfoil. To further explore the changes in the flow field characteristics, the velocity distribution data V near the suction surface of the airfoil are extracted, aiming to observe and analyze the variation patterns of flow velocity at this characteristic location under different cylinder diameter conditions. As shown in Figure 10, the specific characteristic location is at y/C=0.125, and the specific position along the x-direction is represented by the dimensionless ratio x/C relative to the chord length, with the range of x/C being from -0.25 to 1.5.

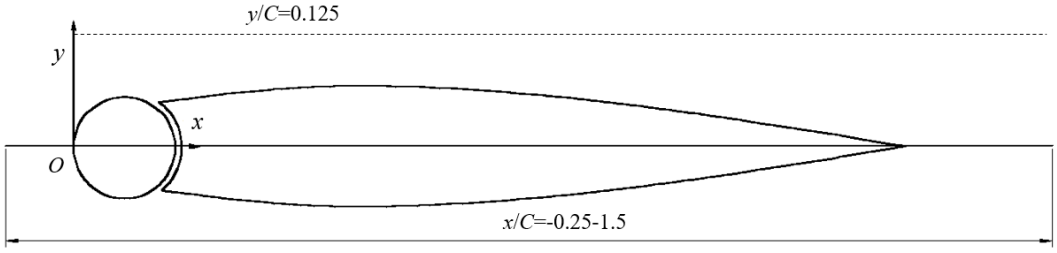

Figure 10. Characteristic position

Figure 11 shows the flow field velocity distribution at the characteristic location y/C=0.125 obtained from the calculations.

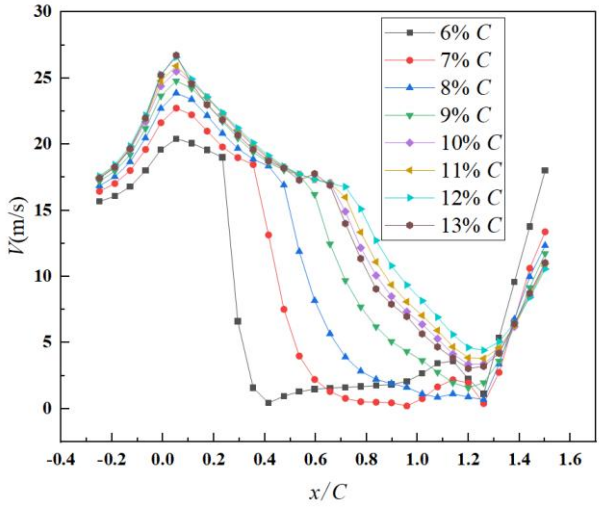

Figure 11. Velocity of x/C from -0.25 to 1.5 at y/C = 0.125

Figure 11 illustrates that, under different cylinder diameter conditions, the velocity distribution near the suction surface of the airfoil follows a distinctive inclined zigzag pattern along the chordwise direction. As the uniform incoming flow passes over the suction surface of the airfoil, the velocity first increases to a peak, then drops sharply. After reaching the minimum velocity, it gradually increases at varying rates. Notably, for all conditions, the position at which the maximum velocity occurs remains consistent, always located at x/C=0.0125. However, the location of the minimum velocity shows significant differences. Specifically, as the cylinder diameter decreases, the position of the minimum velocity shifts closer to the thickest part of the airfoil. In contrast, as the cylinder diameter increases, the minimum velocity moves further towards the trailing edge. When the cylinder diameter reaches or exceeds 8% *C*, the minimum velocity has moved past the trailing edge of the airfoil.At the same time, it is observed that as the cylinder diameter increases, the maximum velocity also increases, though the rate of increase gradually slows. This happens because, for the same rotational speed, a larger cylinder diameter leads to a higher tangential velocity, which has a greater impact on the flow speed. During the process of increasing the cylinder diameter from 6% *C* to 8% *C*, the momentum input from the rotating cylinder has little effect on the minimum velocity, so it remains relatively stable. However, when the diameter increases from 8% *C* to 12% *C*, the momentum input from the rotating cylinder starts to affect the minimum velocity, causing it to increase. But when the cylinder diameter reaches 13% *C*, the diameter becomes too large, causing stronger flow separation, which results in a decrease in the minimum velocity. These observations suggest that the position of the maximum velocity on the suction side of the airfoil is solely dependent on the airfoil shape itself and is independent of the cylinder diameter. In contrast, the cylinder diameter has a significant impact on the position of the minimum velocity and the magnitude of the velocity extremes, although the patterns of influence are not the same.

Specifically, when the cylinder diameter is 6% *C*, the velocity at *x*/*C*=−0.25 near the airfoil leading edge is 15.6 m/s, which is 4% higher than the incoming flow velocity of 15 m/s. This is due to the rotation of the cylinder, which accelerates the surrounding air, and the velocity increases as the distance from the cylinder to the airfoil surface decreases. At *x*/*C*=0.05, the velocity reaches its maximum value of 20.4 m/s, a 36% increase compared to the incoming flow velocity. This indicates that the Magnus effect is strongest near this position, resulting in the maximum velocity at this location. As *x*/*C* increases further, the velocity above the suction surface starts to decrease due to the larger angle of attack, which causes the airflow on the suction side to lose its attached flow, leading to flow separation and the formation of a separation vortex. At *x*/*C*=0.25, the velocity begins to drop sharply because it is close to the separation point, where the velocity change is most dramatic. At *x*/*C*=0.425, the velocity reaches its minimum value of 0.45 m/s, a 97% decrease compared to the incoming flow velocity. After that, as *x*/*C* increases from 0.425 to 1.25, the velocity increases slowly at first and then decreases again, and the velocity remains relatively low. This is due to the flow separation, which creates a low-speed region at the separation point, resulting in lower velocities in this area. From *x*/*C*=1.25 to *x*/*C*=1.5, the velocity continues to rise because at the airfoil trailing edge, a Kármán vortex street phenomenon occurs, and the vortex is positioned higher, allowing the velocity to increase as it moves away from the vortex position.

When the cylinder diameter increases to 7% *C*, the velocity at *x*/*C*=−0.25 is 16.5 m/s, slightly higher than the 6% *C* case. The velocity remains higher than the 6% *C* case up to *x*/*C*=0.5. This is because increasing the cylinder diameter strengthens the Magnus effect, leading to a greater velocity increase around the cylinder. Similarly, at *x*/*C*=0.05, the velocity reaches its maximum value of 22.7 m/s, which is 51.3% higher than the incoming flow velocity. After that, the velocity begins to decrease, reaching a minimum at *x*/*C*=0.35. As *x*/*C* increases further, the velocity drops sharply because the fluid begins to separate. The velocity then enters a low-speed region, fluctuating below 2 m/s, and after moving away from the airfoil trailing edge, at *x*/*C*=1, the velocity starts to recover.

When the cylinder diameter is between 8% *C* and 11% *C*, the velocity at *x*/*C*=−0.25 for all cylinder diameters is greater than the incoming flow velocity, and as the cylinder diameter increases, the velocity at this position also increases. As *x*/*C* increases, the flow field velocity increases as well, and the maximum velocity is reached at *x*/*C*=0.05 for all cylinder diameters. The velocity values increase monotonically with the cylinder diameter. This is because, as the cylinder diameter increases, the Magnus effect of the rotating cylinder intensifies. The larger the cylinder diameter, the greater the velocity at this position. The corresponding maximum velocities are 23.9 m/s, 24.8 m/s, 25.5 m/s, and 25.9 m/s, which are 59.3%, 65.3%, 70%, and 72.7% higher than the incoming flow velocity of 15 m/s, respectively. As *x*/*C* increases, the flow field moves farther from the rotating cylinder, the Magnus effect weakens, and the velocity starts to decrease. However, the rate of decrease is similar for all cylinder diameters. The point at which the velocity decreases sharply differs because, for different cylinder diameters, the corresponding flow field separation points are located differently. Specifically, as the cylinder diameter increases, the momentum input into the flow field also increases, gradually shifting the separation point downstream. For cylinder diameters between 8% and 11% C, no vortex is generated at the rear of the airfoil, so the velocity decreases slowly.

When the cylinder diameter is 12% *C*, the velocity at *x*/*C*=−0.25 is higher than for other cylinder diameters, and as *x*/*C* increases, the velocity for this diameter remains the highest. Additionally, compared to the previous cylinder diameters, the separation point has moved further downstream, and the separation region has shrunk. This results in the highest lift coefficient corresponding to this diameter in Figure 6. Overall, a 12% *C* diameter cylinder better aligns with the airfoil leading edge shape, optimizing the Magnus effect and providing the best control over the boundary layer, leading to the maximum lift coefficient, the minimum drag coefficient, and significantly improved aerodynamic efficiency.

When the cylinder diameter increases to 13% *C*, the velocity at *x*/*C*=−0.25 is lower than for the 12% *C* case, and as *x*/*C* increases, the velocity remains lower than for the 12% *C* case until separation occurs. Compared to the 12% *C* cylinder diameter, the separation point has moved 7.5% of the airfoil chord length upstream. This is

because the further increase in cylinder diameter disrupts the coordination between the cylinder and the airfoil leading edge, affecting the boundary layer development, and causing the separation point to move upstream, increasing the separation vortex. As a result, the lift coefficient decreases compared to the 12% *C* case. After $x/C>1.25$, as the flow moves away from the trailing edge separation region, the velocity starts to increase again.

4. Conclusion

This study investigates the aerodynamic characteristics of a two-dimensional Magnus airfoil at a Reynolds number of $Re=4\times10^5$, using rotating cylinders of varying diameters installed at the leading edge of a NACA0015 airfoil. The analysis employs the *SST* $k-\omega$ turbulence model to derive the lift and drag coefficient curves, as well as the lift-to-drag ratio curves. A comprehensive examination is conducted on the wake vortex structure, pressure distribution, flow field structure, and instantaneous velocity characteristics at key locations. The following key conclusions are drawn:

Installing a rotating cylinder at the leading edge of the airfoil can alter the wake vortex structure. When the cylinder diameter is small, a distinct Kármán vortex street phenomenon is observed. Increasing the cylinder diameter improves the wake vortex structure of the airfoil.

The installation of a rotating cylinder at the leading edge generates a larger negative pressure region in the leading-edge area, effectively delaying flow separation and improving the aerodynamic characteristics of the original airfoil.

Regardless of the cylinder diameter, the flow field velocity reaches its maximum value above the cylinder's center near the leading edge of the airfoil. However, the location and magnitude of the minimum velocity differ with changes in the cylinder diameter, as the flow field separation varies accordingly.

When the cylinder diameter is 12% of the chord length of the NACA0015 airfoil, the Magnus airfoil exhibits the best aerodynamic performance.

In conclusion, this study reveals the nonlinear effects of the rotating cylinder diameter on the flow field characteristics of the Magnus airfoil, providing a solid theoretical foundation for optimizing Magnus airfoil design. By selecting an appropriate cylinder diameter, it is possible to balance the enhancement of the lift coefficient with the suppression of flow separation, thereby optimizing the airfoil's aerodynamic performance. Future research will continue to explore the effects of additional factors, such as cylinder rotational speed ratio, angle of attack, and Reynolds number, on the Magnus airfoil’s aerodynamic characteristics, injecting new vitality into this field of study. In the future, it is necessary to combine 3D multi-physics simulation, multi-airfoil comparison and experimental verification to promote the practical application of this technology in the propulsion of ships with high Reynolds number.

References

1.Zhang C, Zhu J, Guo H, et al. (2024),Technical Requirements for 2023 IMO GHG Strategy, Sustainability, 16(7): 2766.

2.Chen. Li, Peiting. Sun. (2022), Review on the development of marine wing sail assisted propulsion technology, Ship Science and Technology, 44(19):90-96.

3.Modi V J. (1997) Moving Surface Boundary-Layer Control: a Review, J. Fluid Struct, 11(6): 627–663.

4.Modi V J, Munshi S R, Bandyopadhyay G, et al. (1998) High-performance airfoil with moving surface boundary- layer control, J. Aircraft, 35(4): 544-553.

5.Zhang H, Zhu B, Chen W. (2024) Enhancing Energy Harvesting Efficiency of Flapping Wings with Leading-Edge Magnus Effect Cylinder, Biomimetics, 9(5): 293.

6.Haoyun. Deng, Dianzhu. Guan, Senmao. Li, et al. (2023) Influence of Magnus cylinder and variable angle flap on the aerodynamic performance of unmanned sailboat, Chin. J. Ship Res, 18(1): 170-180.

7.Li. Chen. (2007) Experimental Investigation on MovingSurface Boundary Layer Control, National University of Defense Technology, 2007.

8.Junxia. Li , Haihua. Lin, Chengmeng. Sun, et al. (2024) Analysis of aerodynamic performance and application of flettner rotor, J. Inst. Eng. India Ser. C, 105(5): 1373-1383.

9.Chao. Guo. (2023) Numerical Simulation and Optimization Research on Deformation Sail Propulsion of Merchant Ship Based on Magnus, Qingdao University of Science and Technology.

10.Modi V J , Mokhtarian F , Yokomizo T . (2015) Effect of moving surfaces on the airfoil boundary-layer control, J.

Aircraft, 27(1):42-50.

11.Zhou Z, Huang S, Wang Y. (2023) Numerical simulation study of the fluid-structure coupling effects of Kármán vortex street on airfoil motion with varying thickness, Ocean Eng, 286: 115459.

12.Al-Garni A Z, Al-Garni A M, Ahmed S A, et al. (2000) Flow control for an airfoil with leading-edge rotation: an experimental study, J. Aircraft, 37(4): 617-622.

13.Aktharuzzaman M, Sarker M S, Safa W, et al. (2017) Development of an experimental setup for analyzing the influence of Magnus effect on the performance of airfoil, AIP Conf. Proc, 1919(1).

14.Salam M A, Deshpande V, Panday S, et al. (2019) Improvement in aerodynamic performance of NACA0021 airfoil using moving surface boundary layer: A computational study, AIP Conf. Proc, 2121(1).

15.Mohamed M , Abdelsamie A . (2020) Aerodynamic performance improvement using a micro-cylinder as a passive flow control around the S809 airfoil, IOP Conf. Ser.: Mater. Sci. Eng.

16.Yueqing. Zhuang,Diangui. Huang. (2011) Numerical Study on the Aerodynamic Characteristics of the Wind Turbine Airfoil with Rotating Cylinder, J. Eng. Thermophys, 32(1): 43-46.

17.Salimipour E . (2024)On the moving surface impact on flow field and aerodynamic performance of a thick airfoil, Ocean Eng, 291(Jan.1):116504.1-116504.11.

18.Salam M A , Ali M T , (2020) Islam M Q .Experimental Analysis of Aerodynamic Performance on asymmetric NACA 23018 Aerofoil incorporating a Leading-Edge Rotating Cylinder, IOP Conf. Ser.: Mater. Sci. Eng, 912:042027-.

19.Yahiaoui T , Belhenniche M , Imine B ,et al. (2015) Effect of Moving Surface on NACA 63218 Aerodynamic Performance , EPJ Conf, 92:02114.

20.KB R, GANAPATHY SUBRAMANIAN L R. (2024) Aerodynamic study of a leading-edge rotating cylinder in a cambered aerofoil (NACA2412), Aircraft Eng. Aerospace Technol.

21.Gada K, Rahai H. (2016) Lift and Drag Forces of a High Efficiency Airfoil With an Embedded Rotating Cylinder, IMECE, 50619: V007T09A070.

22.Lou B, Huang Z, Ye S, et al. (2020) Experimental and numerical studies on aerodynamic control of NACA 4418 airfoil with a rotating cylinder, J. Vib. Eng. Technol, 8: 141-148.

23.Jixiang. Shan, Xu. Zhang, Qianghong. Chen. (2017) Numerical Simulation on Effects of Rotating Cylinder in Trailing Edge on Airfoil Aerodynamics Characteristic, Comput. Simul, 34(12): 18-21.

24.Zhang Y, Zhao Y. (2023) Novel design of a circulation control airfoil with cylinder rotation, Phys. Fluids, 35(8).

25.Zhang Y, Huang D, Sun X, et al. (2010) Exploration in optimal design of an airfoil with a leading edge rotating cylinder, J. Therm. Sci, 19: 318-325.

26.Xinzi. Tang, Xinyu. Lu, Xiaoyu. Wang, et al. (2021) Numerical Analysis and Optimization of Aerodynamic Performance of Magnus Airfoil at Low Reynolds Number, Acta Energiae Sol. Sin, 42(6):265.

27.Ling. Zhang, Kaixin. Chen, Shengqiang.Gao, et al. (2018) Numerical Simulation on The Magnus Leading Edge Rotating Cylinder Airfoil, Science Technology and Engineering, 18(7).

28.Zhibin. Gong, Jie. Li, Hui. Zhang. (2015) Numerical Simulation on the Effects of Rotating Cylinder on an Airfoil, Acta Aerodyn. Sin, 33(2): 254-258.

Received **03 March 2025**

1st Revised **23 May 2025**

2nd Revised **25 June 2025**

Accepted **01 July 2025**